NASA Technical Memorandum 100938

NASA-TM-100938 19880018711

# As-Received Microstructure of a SiC/Ti–15–3 Composite

Bradley A. Lerch and David R. Hull
*National Aeronautics and Space Administration*
*Lewis Research Center*
*Cleveland, Ohio*

and

Todd A. Leonhardt
*Sverdrup Technology, Inc.*
*NASA Lewis Research Center Group*
*Cleveland, Ohio*

August 1988

NASA

Trade names or manufacturers' names are used in this report for identification only. This usage does not constitute an official endorsement, either expressed or implied, by the National Aeronautics and Space Administration.

# AS-RECEIVED MICROSTRUCTURE OF A SiC/Ti-15-3 COMPOSITE

Bradley A. Lerch and David R. Hull
National Aeronautics and Space Administration
Lewis Research Center
Cleveland, Ohio 44135

and

Todd A. Leonhardt
Sverdrup Technology, Inc.
NASA Lewis Research Center Group
Cleveland, Ohio 44135

## SUMMARY

A silicon carbide (SiC) fiber reinforced titanium (Ti-15V-3Cr-3Sn-3Al) composite is metallographically examined. Several methods for examining composite materials are investigated and documented. Polishing techniques for this material are described. An interference layering method is developed to reveal the structure of the fiber, the reaction zone, and various phases within the matrix. Microprobe and transmission electron microscope (TEM) analyses are performed on the fiber/matrix interface. A detailed description of the fiber distribution as well as the microstructure of the fiber and matrix are presented.

## INTRODUCTION

The development of low-earth-orbit and hypersonic vehicles necessitates the application of high-strength, low-weight materials. This need has spawned large-scale research programs to investigate one of the few possible material systems that can satisfy such requirements: composite materials. The Advanced High Temperature Engine Materials Technology Program at NASA Lewis Research Center is one of these programs. This program will develop the technology needed to apply composite materials to high-performance propulsion systems. This program involves both the Materials and Structures Divisions and will provide guidance for composite development from the fabrication of the composite constituents to structural analysis methodologies.

In support of this program, a commercially available SiC/Ti-15V-3Cr-3Al-3Sn (henceforth called SiC/Ti-15-3) composite is being researched. Although titanium alloys are not generally thought of as high-temperature materials, this alloy is believed to exhibit some of the characteristics of future high-temperature composite systems. Thus, this alloy acts as a model for more advanced composites, enabling the necessary technology to be currently developed. As the more advanced, high-temperature composites become available, an easier transition can be made with minimal setup time.

The change from monolithic materials to composites research introduces a variety of new and complex problems. Even simple procedures such as specimen cutting and metallographic preparation become a challenge with composite materials. The purpose of this report is twofold: (1) to investigate and document

some of the common metallographic techniques that can be used for composite materials and (2) to document the initial micro- and macrostructure of the SiC/Ti-15-3 material to provide guidance for the structural mechanics modeler.

## EXPERIMENTAL PROCEDURE

### Optical Microscopy

All specimens were sectioned by using a 0.30-mm-thick diamond-impregnated (320 mesh, high diamond concentration), thin-sectioning wheel and mounted in an epoxy resin. The specimens were prepared with automated metallographic equipment such as that described in reference 1. A resin-bonded, 115-μm diamond grinding disk was used to grind the specimens flat. Subsequent diamond grits of 65 and 26 μm were used for finer grinding. In all cases, a 20-kPa head pressure was applied to the specimens. The grinding disk velocity was 150 rpm, and water was used as a lubricant.

After the final grinding, the specimens were lapped on a copper-iron-epoxy composite lapping disk, which had been sprayed with a 6-μm diamond slurry. The head pressure and wheel velocity were the same as in the grinding operations; however, an alcohol-based lubricant was used instead of water. After 4 min, additional lapping was done on polymeric lapping disks with a 6-μm diamond slurry and subsequently with a 3-μm diamond slurry.

Refinement of the microstructure required polishing with fine diamond. This was accomplished on a hard synthetic cloth with 1-μm diamond abrasive. The polishing parameters were similar to those in lapping, except that the head pressure was increased to 30 kPa. Final polishing was performed for 4 to 24 hr on a vibratory polishing machine by using 0.5-μm diamond paste and ethyl glycol applied to a synthetic velvet cloth. Selected specimens were etched with a solution of 100 ml $H_2O$, 6 ml $HNO_3$, and 3 ml HF.

Selected specimens were coated with an interference layer to allow easy differentiation between phases. The interference layer was applied at a 2-mbar partial pressure of oxygen with the specimen located 15 to 20 mm from a chilled platinum target. The cathode current was 50 to 55 mA and was applied for 200 sec. These conditions provided an interference layer which appeared light blue in color at a magnification of 1X.

### Scanning Electron Microscopy (SEM)

Polished specimens were examined at accelerating voltages of 15 and 20 kV in the as-polished, etched, or interference-layered conditions. Elemental x-ray analysis involving spot modes, analog line scans, and dot mapping was performed as necessary.

### Transmission Electron Microscopy (TEM)

Rectangular rods 3 by 2 by 10 mm were sectioned from a composite coupon by using a thin-sectioning diamond wheel. The specimen corners were ground on a 65-μm (220 grit) diamond wheel until the maximum diagonal dimension was less than 3 mm. TEM blanks having a thickness of 0.3 to 0.5 mm were cut from these rods perpendicular to the fibers by using a diamond wheel. They were ground to

a thickness of 200 μm with 6-μm diamond lapping films. The blanks were subsequently dimpled by using a 16-mm-diameter by 1.5-mm-thick rotating brass wheel, which was coated with a 15-μm diamond slurry. Ninety micrometers of material was removed from each side of the blank. The final 10 μm of material removal on each side was performed by using a 3-μm diamond slurry. The dimpling procedure was stopped shortly before perforation of the foil by the brass wheel. Thereafter, the dimpled foils were ion-beam milled at 5 kV and at a gun current of 0.4 mA. The foils were inclined ~10° to the ion beam. Cooling the specimen with liquid nitrogen was found necessary to ensure a more uniform thinning rate of all the constituents. This process required about one day to thin a foil that was suitable for viewing in the TEM at 120 kV.

## RESULTS

### Macrostructure

The composite was received in sheet form with a nominal thickness of 2 mm. The material was consolidated by AVCO Specialty Metals Division under a proprietary process. Alternate layers of SiC fibers (SCS-6) and foils of Ti-15-3 were hot-pressed to yield sheets consisting of eight layers of fibers and nine layers of titanium alloy foil in a unidirectional layup. A typical cross section showing this layup can be seen in figure 1. There appeared to be no porosity, and the fiber distribution was relatively uniform. The average fiber volume fraction, measured by using the point intercept count method (ref. 2), was found to be 36 percent. Fiber-center-to-fiber-center distance within a row varied from 145 μm (i.e., the fibers were touching) to about 290 μm. In the case of touching fibers,there was always a crack at the point of tangency, as depicted in figure 2. Since large amounts of inhomogeneous flow occurred in the matrix during consolidation, the fiber centers in any row varied about an average centerline by a maximum of about 50 μm. An average separation between the centers of any two fiber rows was measured as 350±20 μm. These dimensions yield an array of fibers which can be simulated for modeling purposes as a rectangle (fig. 1) having corners at the fiber centers and having average edge lengths of 220 μm parallel to the fiber rows and 350 μm perpendicular to the rows.

### Microstructure

Matrix. - The Ti-15-3 matrix was received in the annealed state. It consisted primarily of the metastable β-Ti phase. This phase has a body-centered cubic (bcc) crystal structure having a lattice parameter of 3.226±0.002 Å as measured by x-ray diffraction. Analysis of the chemical composition of the matrix by a plasma arc technique yielded the following contents in weight percent: Ti, 77.7; V, 13.2; Al, 3.2; Cr, 3.1; Sn, 2.6; and Fe, 0.2. The grain structure is shown in figure 3. The grains are generally orthorhombic in shape, having boundaries both parallel and perpendicular to the fiber rows. The boundaries are relatively straight and appear to be free of any particles. Between fibers within a row, there are often smaller grains. An average grain size measurement was not performed because of the irregular shape of the grains. A reasonable description of the grain size for modeling purposes would be grains of orthorhombic shape having one dimension equal to the spacing between the fiber rows (350 μm), another dimension about half of the fiber

spacing within a row (110 μm), and the remaining dimension parallel to the fiber axis (200 μm).

Within each large grain, a substructure can be seen (fig. 4), the boundaries of which are decorated by a second phase. The second phase also precipitated within the small grains (fig. 4). When viewed at a lower magnification (fig. 3), it appears that this phase is restricted to the matrix between fiber rows.

An examination of a specimen which had been sectioned parallel to the fibers revealed a distribution of small equiaxed grains immediately surrounding the fibers. This can be readily observed in figure 5 in an area just below a fiber (i.e., where the fiber has been polished away to reveal the matrix directly below it). The grain diameters in this area range from 10 to 80 μm. Numerous particles ~3 μm in size could be observed in the grain boundaries as well as in the grain interiors. The horizontal line in figure 5 is the laminae boundary.

One of the middle fiber rows in figure 3 exhibits a darkened area weaving around the fibers. This occurred to some extent in at least one fiber row in each metallographic mount. A higher magnification (fig. 6) depicts the fine structure of such an area. The large white particles that connect the fibers were shown to be rich in Ti and C by SEM x-ray energy dispersive (XEDS) and wavelength dispersive (WDS) spectroscopy. This implies that they were TiC. Between the TiC particles is an acicular phase, which, on the basis of optical microscopy and XEDS analysis, is believed to be an $\alpha$-$\beta$ structure. The dark phase was examined by using a standardless elemental x-ray analysis. The results are shown in table I for the dark area and for the matrix. It can be seen that the dark areas contained lesser amounts of Al, V, Cr, and Sn, but more Ti than the matrix.

Fiber. - The SiC (SCS-6) fiber was manufactured by Avco Specialty Metals Division. It was produced by a chemical vapor deposition (CVD) process which has been described elsewhere (refs. 3 and 4). The fiber is a complex, multilayered structure (fig. 7), which starts as a 33-μm-diameter carbon monofilament at the center of the fiber (region 1). A pyrolytic carbon coating was deposited on the carbon core (ref. 3) up to a thickness of 1.5 μm (region 2). This coating consists of feathery grains, which are elongated in the radial, or growth, direction. Silicon carbide is deposited upon this substrate. At the interface of the pyrolytic carbon coating and the SiC (fig. 8), the SiC forms first as small equiaxed crystallites having a diameter of ~0.03 μm. As the SiC grows, the grains become elongated (fig. 8) in the radial direction (region 3). At 21 μm from the pyrolytic coating, there is a change in structure (fig. 7). At this point the SiC grain diameter increases by about a factor of three (region 4). From this transition to the outer radius of the SiC, the fiber consists of large elongated grains, as shown in the TEM image in figure 9(a). The grains are heavily faulted, and this gives rise to streaks in the corresponding electron diffraction pattern (fig. 9(b)). Also shown in the diffraction pattern is an asterism, which is indicative of slight misorientations between the grains. The {111} diffraction spots are parallel to the growth direction, and the asterism in these spots indicates that not all grains have

perfectly parallel <111> directions. An enlargement of a single SiC grain is depicted with dark field imagery in figure 10(a). The [011] diffraction pattern (fig. 10(b)) indicates that a $[\bar{1}11]$ direction is parallel to the long dimension of the grain. The $(\bar{1}11)$ fault planes are seen in the edge-on condition.

At the outer radius of the SiC fiber is a 3-μm-thick coating (region 5 in fig. 7). In both optical (fig. 7) and TEM micrographs (fig. 11) the coating appeared to consist of two layers. However, on closer inspection region 5 consists of several zones, which have been numbered to correspond to the notation of Nutt and Wawner (ref. 5). Zone I (fig. 11) forms on the SiC and is 0.05 to 0.06 μm thick. Zone II is 0.65 to 1.10 μm thick and contains small crystallites. The third zone consisted primarily of an amorphous layer. A diffraction pattern of zone III (fig. 12) showed diffuse rings with no preferred orientation. This zone ends at the definitive boundary observed in both figure 11 and in the optical micrograph (fig. 7). Zone IV extends from this boundary to the reaction zone, a distance of about 0.85 μm. Small crystallites can also be observed in zone IV.

X-ray elemental analyses for silicon content using TEM were performed at various locations within this coating. Fourteen analyses were taken across the coating. The diameter of the area being analyzed was approximately 0.08 μm. The results are presented in figure 13. The bright field micrograph (lower photo) and the graph have a one-to-one correspondence so that the silicon content at individual locations in the coating can be easily correlated. These results are qualitative, indicating only relative changes in the silicon content. Changes in the composition are also assumed to be a result only of the actual change in silicon content and not changes in the foil thickness. An increase in the volume of material being analyzed (i.e., thicker foil) will result in the emission of more x-rays (ref. 6), and the material will appear to have a higher silicon content. No obvious thickness change was observed within this coating because of the lack of intensity variations in the negative. However, it was noticed that the SiC was thinner (less x-ray emission), and the matrix thicker (more x-ray emission), than the coating.

The elemental analysis indicates that three silicon-rich zones are present within the coating. The first occurred at the SiC coating interface (zone I). The Si content dropped sharply as zone II began and remained constant throughout zone II. An increase in Si started with the beginning of zone III and continued to increase to a maximum at the interface of zones III and IV. A sharp drop in Si at this interface was followed by a gradual increase of Si in zone IV as the reaction zone was approached.

A reaction (region 6) formed at the interface between zone IV and the titanium matrix. This reaction zone had a thickness of 0.10 to 0.35 μm. Its distance from the outer diameter of the SiC varied greatly, probably depending on the original roughness of the zone IV coating. The reaction zone was composed of tiny crystallites having dimensions on the order of 0.01 to 0.2 μm (fig. 14(a)), which gave rise to a very complex diffraction pattern (fig. 14(b)). Smaller crystallites were located at the coating side of the reaction zone, while larger, more widely separated particles were observed on the matrix side. A dark field micrograph imaged with a diffraction spot from a particle at the coating side of the reaction zone is shown in figure 15. The

same diffraction spot also imaged very fine particles within zone IV of the carbon-rich coating.

To reveal compositional differences at the fiber/matrix interface, a microprobe analysis was performed for the following elements: Ti, V, Cr, Al, C, Si, and O. A qualitative analysis was done in the form of an analog line scan. The relative changes in the element concentrations were recorded as the electron beam moved across the specimen. The examined specimen was cut longitudinally (almost parallel to the fibers) so that the thickness of the coating/reaction zone could be exaggerated. Since the probe size was larger than the coating thickness, the composition of several zones was averaged, reducing the ability to define small elemental differences. Nevertheless, large compositional changes were observed. The trace of the beam is depicted in figure 16. Plots of x-ray intensity (which is proportional to the amount of the element present) with respect to position is given in figure 17. For ease of representation the original plots were smoothed and all background noise removed. No correction was made for absorption. The vertical scale for each individual element, is different, and therefore element-to-element intensities cannot be compared. However, significant changes in composition for any one element can be estimated by comparing the change in intensity to the weight percent of that particular element at its maximum value (i.e., the amount in the matrix or in the fiber). Also, oxygen was not represented in these plots since the measured amount of oxygen did not vary at any location above the background (i.e., no oxygen segregation).

Plots of the microprobe data are separated into two elemental groups: (1) Si, C, Ti (fiber constituents, fig. 17(a)) and (2) Ti, V, Cr, Al (matrix constituents, fig. 17(b)), where Ti serves as a cross reference. In figure 17(a) the carbon extends well into the reaction zone, slowly decreasing to its value in the matrix. Silicon, on the other hand, peaks inside the reaction zone near the matrix. The matrix elements Ti, V, and Cr show an increase at the interface of zone IV and the reaction zone (fig. 17(b)). In the reaction zone Cr, V, and Al show large variations and a steady increase until the matrix is reached. At that point the levels of all elements become constant.

## DISCUSSION

### Macrostructure

The integrity of the SiC/Ti-15-3 composite material was generally good. There were no observed pores or voids nor were there regions of unbonded areas either at the fiber/matrix interface or at the interface between laminae. There were occasional fibers containing very fine radial cracks (not necessarily associated with touching fibers) which normally were visible only upon etching. However, it is not known if the cracks were a result of fabrication or due to metallographic preparation.

On the basis of the macrostructural observations, a model array of fibers within the matrix was suggested. The array consisted of a rectangle with fiber centers at the corners. The edge lengths were 220 μm parallel to the fiber rows and 350 μm perpendicular to the rows. This array simulates the actual

macrostructure fairly well since the distance between fiber centers perpendicular to the rows did not vary by more than 10 percent. There was a larger variation between fiber centers within a row since the center-to-center distance varied by about a factor of two. The most severe case resulted when the fibers touched (fig. 2). This led to cracking of the fiber coating and occasional debonding of the coating within the area of contact. An examination of 1600 fibers indicated that 6.3 percent of the fibers touched or were close enough to one another to induce coating cracks. (Note: this number counts only one of the pair of touching fibers.) Touching fibers have been shown in other metal matrix composites to be a weak spot degrading the composite properties (refs. 7 and 8). Although the fiber separation is nonuniform within a row, the general distribution of fibers is much better than that observed in composites fabricated by using a liquid infiltration method. In these cases fibers often form clusters in which many fibers touch and large areas of matrix are not reinforced (refs. 7 and 8).

## Microstructure

Matrix. - The grain structure in this material is unusual in that the grains are orthorhombic in shape, although there are some grains which are more equiaxed. The grains in this composite appeared to have grown to the extent of the original Ti-15-3 foil thickness. This is typical for grain growth in thin sheets in which the grains grow across the thickness of the sheet (ref. 9). The internal grain boundaries are perpendicular to the free surface; this minimizes the boundary area. During hot-pressing of the composite, the grains should be capable of further growth across the laminae. The movement of the horizontal boundaries is restricted because of the presence of fine particles at the interlaminae surface (fig. 5). These particles probably form from organics (e.g., dirt) on the surface of the laminae, which are not removed before consolidation. There are some instances where grains traverse the laminae boundaries, but this seldom occurred.

Immediately surrounding the fibers are finer, more equiaxed grains (fig. 5). These grains have sizes in the range 10 to 80 μm and are probably a result of recrystallization during fabrication. During consolidation there is a large amount of viscoplastic flow in the region of the fibers. This is necessary to ensure complete bonding. The high strains probably produce large dislocation densities in these areas, which should provide a sufficient driving force for the recrystallization process. Further grain growth in this area is inhibited because of the large number of particles (fig. 5). These particles are outlying portions of the reaction zone.

The small grains may present problems at elevated temperatures. Since creep rates are inversely proportional to the grain diameter, this area around the fibers will creep faster than the surrounding matrix and as such could absorb large amounts of strain. Smaller grains also have more grain boundary area per unit volume, providing additional paths for oxygen diffusion and embrittling the interface region. This weakened area, coupled with the high stresses at the interface due to differences in properties between the matrix and the fiber, make this a weak link in the composite.

Occasionally observed were areas of what appeared to be particles woven around the fibers (figs. 3 and 6). Titanium wires are woven between the SiC at

approximately 5-mm intervals along the fiber length to keep the fibers parallel during fabrication. The large white particles in figure 6 were a result of this reaction. Chemically analyzed with the SEM and found to be high in Ti and C, these particles are probably TiC. The solubility of C in Ti is very low (ref. 10), and therefore little C is required to form these particles. The small particles between the laminae (fig. 5) are also suspected to be TiC as determined by their color due to interference layering.

In the matrix between the woven carbides was a coarse lamellar structure. Since no major compositional differences were observed between the two lamellar phases, this structure is believed to be $\alpha$-$\beta$ Ti. The coarse lamellae are reportedly a result of very slow cooling (ref. 10). Surrounding the woven carbides was a dark phase (fig. 3). Elemental analysis indicated this area to be lean in V, Al, Cr, and Sn, but rich in Ti compared to the matrix. No other differences were observed between the matrix and this phase. On the basis of the chemical analysis and its appearance, the dark area is believed to be the $\beta'$-phase. The $\beta'$-phase is a solute lean, coherent, bcc zone which forms where precipitation of the $\alpha$-phase is sluggish (ref. 11). It has been observed in several $\beta$-Ti-alloys (refs. 11 to 13).

Fiber. - The SCS-6 fiber was produced by a CVD process in which SiC is deposited on a carbon core monofilament. On this core is a layer of pyrolytic graphite which provides a uniformly smooth surface on which the SiC can be deposited (refs. 3 and 5). This coating has feathery grains elongated in the growth, or radial, direction (fig. 8). The prime constituent of the fiber is SiC. A carbon-rich coating is deposited upon the SiC to yield a final fiber radius of 145 $\mu$m. The carbon coating is applied to increase the strength of the fiber, primarily by reducing surface flaws (ref. 3).

Three grain sizes of SiC exist within the fiber. The first is immediately adjacent to the pyrolytic carbon layer and has a small equiaxed grain size of 0.03 $\mu$m (fig. 8). As the SiC was further deposited, the grains increased in size and assumed an elongated shape. The long dimension of the grains was parallel to the growth direction and had an aspect ratio of about 10. This grain size remained constant until about halfway through the SiC, where a distinct change can be observed (fig. 7). This is due to a change in grain size of the SiC, resulting from a variation in the deposition gases during the CVD process (refs. 4 and 5). The grains are larger in the outer half of the fiber.

The fiber is composed of the $\beta$-SiC phase (refs. 3 to 5) which has a face-centered cubic (fcc) crystal structure (ref. 14). A detailed description of this structure is given in refs. 4 and 5, and only a few pertinent details will be mentioned here. The grains have a preferential growth direction of $\langle 111 \rangle$ (figs. 9 and 10), which is parallel to the long dimension of the grain. However, the grains are not all perfectly parallel. The slight misorientation gives rise to an asterism in the $\{111\}$ diffraction spots, as depicted in figure 9(b). The lines running perpendicular to the growth direction are stacking faults (refs. 4, 5, 14, and 15). In the dark field image in figure 10(a) the grain normal is parallel to an $[01\bar{1}]$ direction, and the faults are observed edge-on (ref. 5). Disturbances in the stacking sequence give rise to the various streaks shown in the diffraction patterns in figures 9(b) and 10(b).

The various sections of the SCS-6 fiber are difficult to discern in the as-polished state. Etching is difficult to do and requires heating to 500 °C

(ref. 4), which is abusive to the matrix. Normal acid etches to reveal matrix structures are not sufficient to reveal the fiber details. However, the interference layering technique did accentuate small contrast differences, and it permitted identification of each individual zone. In this process, a thin layer of Pt is deposited on the surface of the specimen. Differences in the reflection of light at the metal/Pt, Pt/air interface result not only in a contrast enhancement, but in a color separation for each phase. The particular colors which form and the magnitude of the contrast depend on the optical constants of the phases in the substrate and in the Pt layer. A detailed explanation of this effect can be found in reference 16. Figure 7 is a micrograph of an interference-layered specimen revealing distinctly the carbon core, the pyrolytic coating, the midradius grain size change, the individual coatings on the fiber surface, the reaction zone, and various matrix features. Each area appeared as a different color or shade of color when viewed under visible light. This process is ideal for highlighting phase differences in metal matrix composites, which can be observed by using optical microscopy or SEM. The coating is quickly applied and can be removed with a cotton swab and alcohol. In contrast, the removal of an etch must be done by repolishing the specimen, a time-involved process for these composites.

The SCS-6 fiber was developed primarily for reinforcing titanium alloys (ref. 3). The carbon-rich coating on the outer diameter of the fiber was tailored not only to improve the strength of the fiber, but to control the fiber-matrix reaction. It has a Si content which exhibits a maximum halfway through the coating and at the outer surface of the coating. This was confirmed with the microprobe analysis (fig. 17) as well as with the TEM analysis (fig. 13). It appeared, however, that the first Si maximum occurred at ~2.2 μm from the SiC (fig. 13) rather than at 1.5 μm, as suggested in reference 3. This peak corresponded to the salient change in the coating structure, which was evident even in optical micrographs. The line separating these two structures always appeared ~2/3 of the way to the surface of the coating. This can also be seen in the longitudinally cut fibers (fig. 16). Also associated with the change in grain size is a change in the optical properties of the SiC. When TEM thin foils were viewed under transmitted light, the outer portion (large-grained SiC) of the fiber was transparent, but the inner portion (small-grained and equiaxed-grained SiC) as well as the carbon core were opaque. The transparency indicates high purity in the outer portion of the fiber (ref. 17).

Several zones within this coating have been identified in reference 5 for an SCS-2 fiber. Although these fibers have a slightly different coating than that of the SCS-6 fiber used in this study, the numbering scheme in reference 5 has been adopted in this report (fig. 11). Zone I is the thin layer adjacent to the SiC. This layer consisted of small particles of SiC in a carbon matrix. This would be consistent with the high Si content observed in figure 13. As zone II is traversed, the amount of SiC crystallites declined although the Si content remained constant. Zone III is basically featureless and appeared to exist entirely of amorphous carbon (see diffraction pattern in fig. 12). No SiC crystals could be observed, nor was there any evidence of a preferred orientation as was reported for SCS-2 fibers (ref. 5). After the abrupt microstructural change, zone IV again showed evidence of tiny crystallites. These are believed to be TiC particles and will be discussed further in the following paragraphs.

On consolidation the matrix reacts with the fiber coating to form a reaction product. This product transfers load from the fiber to the matrix, and

the quality of the bond between the reaction zone and either the fiber or the matrix ultimately determines the properties of the composite (ref. 18). By using TEM micrographs the reaction zone in this material was measured to be 0.10 to 0.35 μm thick. The reaction zone size of other SiC/Ti composites is usually larger than 1 μm (refs. 19 and 20) and can be as large as 15 μm (ref. 21). In a few cases the size was 0.35 μm (ref. 22). The extremely small size of the reaction zone made it difficult to examine. Also, during thinning of the TEM foils the reaction zone was the first material to be thinned away, thus greatly extending the time needed to produce a foil in which the matrix, carbon coating, and SiC fiber could be viewed simultaneously.

The reaction zone consisted of small crystallites, those next to the carbon coating having 0.01-μm diameters and those adjacent to the matrix having 0.1- to 0.2-μm diameters. The reaction zone is not a continuous layer or film as suggested by the SEM and optical micrographs (figs. 7 and 16). Because of the fineness of the particles, several of them were analyzed within the selected area aperture at one time. This yielded a diffraction pattern such as that observed in figure 14(b). A multitude of spots present as a result of numerous grain orientations and various crystal structures made identification of the particles impossible by conventional diffraction techniques. An accurate identification of the particles could only be done with convergent beam microscopy in which the beam could be focused to 0.04 μm. However, analysis of this type is extremely time consuming and was not deemed worthwhile for the present study.

Chemical analysis of the reaction zone using microprobe and XEDS analyses revealed sufficient information to estimate the actual composition of the constituents. The prime constituents of the reaction zone were Ti and C (probably TiC). This can be observed in the microprobe analysis in figure 17. At the carbon-rich coating (zone IV) interface there was a high C content. There were also small peaks of V and Cr at this interface. As the reaction zone was traversed in a direction toward the matrix, the C content decreased, and Si, V, Cr, and Al increased. Scanning transmission electron microscopy (STEM) analysis also indicated a high concentration of Si near the matrix. The XEDS results suggested that the particles adjacent to the carbon-rich coating are TiC. The Cr and V peaks in this area suggested that they may substitute in small amounts for the Ti. The small particles imaged by dark field microscopy within zone IV (fig. 15) of the carbon-rich coating are also believed to be TiC (because of the high concentrations of Ti and C). This indicates that Ti has diffused into the coating. Nutt and Wawner (ref. 23) have reported small crystallites in zone IV of the carbon-coating to be SiC. Because of the small size of these particles, an exact identification could not be made. However, the much greater amount of Ti than Si in this area lends support to the presence of TiC. On the matrix side, the reaction products were composed of Ti and Si and therefore were presumed to be titanium silicides, although once again other elements may substitute for Ti. At the tip of the reaction zone in figure 16 there were islands of reaction products dispersed within the matrix. Alternating areas of matrix and reaction zone result in the peaks observed for V, Cr, and Al in figure 17(b).

Other researchers (refs. 19, 20, and 24) have identified reaction products in other SiC/Ti composites to be TiC and $Ti_5Si_3$. Dudek et al. (ref. 19) identified three zones within the reaction products by using Auger spectroscopy. The small particles near the fiber were TiC, the larger particles near

the matrix were $Ti_5Si_3$, and the particles in the middle were a mixture of both. TiC and $Ti_5Si_3$ were also observed in the reaction zone in a titanium aluminide composite (ref. 24). Rhodes and Spurling (ref. 20) found three similar zones in Ti-6Al-4V reinforced with SiC (SCS-6) fibers. However, the composition was slightly different from that found by Dudek et al. (ref. 19). Using convergent beam microscopy, Rhodes and Spurling (ref. 20) identified a layer of TiC and $Ti_5Si_3$ adjacent to the carbon-rich coating, TiC in the middle of the reaction zone, and $Ti_5Si_3$ next to the matrix. They observed no participation of Cr or V in the reaction products; however, this is contrary to that observed in this investigation.

## SUMMARY OF RESULTS

The as-received structure of the SiC/Ti-15-3 composite system was investigated by using various metallographic techniques. A summary of the more pertinent microstructural features is listed as follows:

1. The SiC (SCS-6) fiber distribution within the matrix approximated a rectangular array. Average fiber center-to-center distances were 220 μm within a row and 350 μm between rows. Fiber separation within any row varied greatly. Out of 1600 fibers, 6.3 percent of them touched and always contained coating cracks at the point of tangency. The fiber volume fraction was measured as 36 percent.

2. The grains within the matrix were generally orthorhombic in shape with an average dimension of 200 μm parallel to the fibers and with lengths of 110 and 350 μm in the transverse plane.

3. A series of small, more equiaxed grains of diameters in the range 10 to 80 μm surrounded the fibers.

4. Titanium wires were woven around the fibers to keep them parallel during fabrication. Upon consolidation the wires formed particles which were high in Ti and C (probably TiC). Between the particles was a lamellar structure which was believed to be α- and β-Ti. The matrix surrounding this woven structure had appeared to transform to the solute lean β'-phase.

5. The fibers were composed of a carbon core, upon which a pyrolytic carbon coating was deposited. SiC was built up on this core by using a chemical vapor deposition (CVD) process. Small equiaxed grains were observed adjacent to the pyrolytic coating. The SiC grains became elongated as the fiber diameter increased. The grains were heavily faulted.

6. An interference layering technique was developed which permitted easy identification of the various fiber regions.

7. A carbon-rich coating was applied to the fiber surface. Four zones were identified within this coating. The composition and structure of each zone were identified.

8. A reaction zone 0.10 to 0.35 μm thick formed at the interface between the matrix and the fiber. This zone consisted of very small crystallites,

which were believed to be TiC at the fiber side and $Ti_5Si_3$ at the matrix side of the reaction zone.

## REFERENCES


1. Weidmann, E.: Metallographic Preparation of Metal Matrix Composites and Ceramic Coatings for Microstructural Analysis. Metal Matrix, Carbon, and Ceramic Matrix Composites, 1986. NASA CP-2445, J.D. Buckley, ed., 1986, pp. 93-100.

2. Underwood, E.E.: Quantitative Stereology. Addison-Wesley Publishing Co., Reading, MA, 1970, pp. 1-30.

3. Marzik, J.V.: CVD Fibers. Proceedings of the Metal and Ceramic Matrix Composite Processing Conference, MCMC-1, Metals and Ceramics Information Center, Battelle Labs, Columbus, OH, Nov. 1984.

4. Wawner, F.W.; Teng, A.Y.; and Nutt, S.R.: Microstructural Characterization of SiC (SCS) Filaments. SAMPE Q., vol. 14, no. 3, Apr. 1983, pp. 39-45.

5. Nutt, S.R.; and Wawner, F.E.: Silicon Carbide Filaments: Microstructure. J. Mater. Sci., vol. 20, no. 6, June 1985, pp. 1953-1960.

6. Bolon, R.B.; Lifshin, E.; and Ciccarelli, M.F.: Microanalysis of Thin Films and Fine Structure. Practical Scanning Electron Microscopy, J.I. Goldstein and H. Yakowitz, eds., Plenum Press, 1975, pp. 299-326.

7. Tsangarakis, N.; Slepetz, J.M.; and Nunes, J.: Fatigue Behavior of Alumina Fiber Reinforced Aluminum Composites. Recent Advances in Composites in the United States and Japan, ASTM STP-864, J.R. Vinson and M. Taya, eds., ASTM, 1985, pp. 131-152.

8. Shetty, H.R.; and Chou, T.W.: Mechanical Properties and Failure Characteristics of FP/Aluminum and W/Aluminum Composites. Metall. Trans. A, vol. 16, no. 5, May 1985, pp. 853-864.

9. Cotterill, P.; and Mould, P.R.: Recrystallization and Grain Growth in Metals. John Wiley and Sons, 1976.

10. Ogden, H.R.; and Holden, F.C.: Metallography of Titanium Alloys. BMI-TML-103, Battelle Memorial Institute, Columbus, OH, May 1958.

11. Williams, J.C.: Critical Review Kinetics and Phase Transformations. Titanium Science and Technology, Vol. 3, R.I. Jaffee and H.M. Burte, eds., Plenum Press, 1973, pp. 1433-1494.

12. Ankem, S.; and Seagle, S.R.: Heat Treatment of Metastable Beta Titanium Alloys. Beta Titanium Alloys in the 80's, R.R. Boyer and H.W. Rosenberg, eds., Metallurgical Society of AIME, Warrendale, PA, 1984, pp. 107-126.

13. Rhodes, C.G.; and Paton, N.E.: The Influence of Microstructure on Mechanical Properties in Ti-3Al-8V-6Cr-4Mo-4Zr (Beta C). Metall. Trans. A, vol. 8, no. 11, Nov. 1977, pp. 1749-1761.

14. Shinozaki, S.S.; and Sato, H.: Microstructure of SiC Prepared by Chemical Vapor Deposition. J. Am. Ceram. Soc., vol. 61, no. 9-10, Sept.-Oct. 1978, pp. 425-429.

15. Ogbuji, L.U., et al.: The $\beta$-$\alpha$ Transformation in Polycrystalline SiC: IV, A Comparison of Conventionally Sintered, Hot-Pressed, Reaction-Sintered, and Chemically Vapor-Deposited Samples. J. Am. Ceram. Soc., vol. 64, no. 2, Feb. 1981, pp. 100-105.

16. Buehler, H.E.; and Hougardy, H.P.: Atlas of Interference Layer Metallography. Deutsche Gesellschaft fuer Metallkunde, Oberursel, W. Germany, 1980.

17. Powell, J.A.: Silicon Carbide, a High Temperature Semiconductor. NASA TM-83514, 1983.

18. Chou, T.W.; Kelly, A.; and Okura, A.: Fibre-Reinforced Metal-Matrix Composites. Composites, vol. 16, no. 3, July 1985, pp. 187-206.

19. Dudek, H.J.; Leucht, R.; and Ziegler, G.: Auger Electron Spectroscopy of the Interface of SiC Fiber Reinforced Titanium Alloys. Titanium: Science and Technology, vol. 3, Deutsche Gesellschaft fuer Metallkunde, Oberursel, W. Germany, 1985, pp. 1773-1780.

20. Rhodes, C.G.; and Spurling, R.A.: Fiber-Matrix Reaction Zone Growth Kinetics in SiC-Reinforced Ti-6Al-4V as Studied by Transmission Electron Microscopy. Recent Advances in Composites in the United States and Japan, ASTM STP-864, J.R. Vinson and M. Taya, eds., ASTM, Philadelphia, 1985, pp. 585-599.

21. Ziegler, G.; Dudek, H.J.; and Bunk, W.: Contribution to the Development of Fiber-Reinforced Titanium Alloys (Beitrag zur Entwicklung von faserverstaerkten Titanlegierungen). Proceedings of the 7th International Leichtmetalltagung, Leoben, Austria, 1981, pp. 204-205.

22. Brewer, W.D.; and Unnam, J.: Interface Control and Mechanical Property Improvements in Silicon Carbide/Titanium Composites. NASA TP-2066, 1982.

23. Nutt, S.R.; and Wawner, F.E.: Characterization of the Surface Layer on SiC Filaments. Metal Matrix Composites II, NASA CP-2252, J.D. Buckley, ed., 1982, pp. 27-42.

24. Baumann, S.F.: Characterization of Reaction Zone in NASA's Ti-24Al-11NB/SCS-6 Composite (As-Consolidated Condition). Internal Report, Alloy Technology Division, Alcoa Technical Center, Alcoa Center, Pa., Dec. 1987.

TABLE I. - STANDARDLESS X-RAY ANALYSIS OF DARK PHASE AND MATRIX SURROUNDING WOVEN Ti WIRE

| Element | Composition, wt % | |
|---|---|---|
| | Matrix, β | Dark phase, β' |
| Ti | 71.6 | 76.9 |
| V | 13.8 | 10.5 |
| Al | 7.2 | 6.4 |
| Cr | 2.6 | 2.1 |
| Sn | 4.9 | 4.1 |

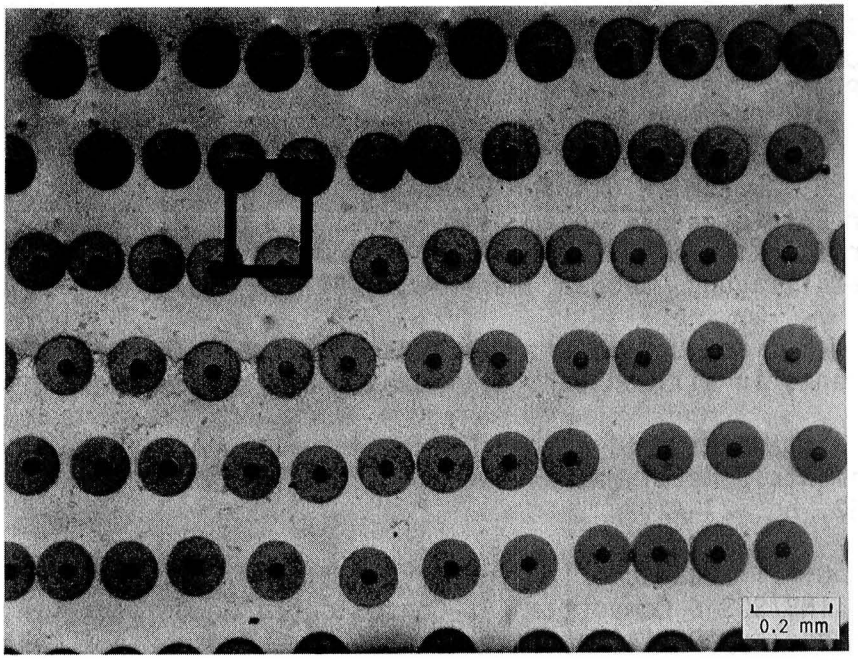


FIGURE 1. - FIBER DISTRIBUTION IN SiC/Ti-15-3 COMPOSITE (AS-POLISHED). RECTANGLE INDICATES MODEL ELEMENT FOR DESCRIBING FIBER ARRAY.

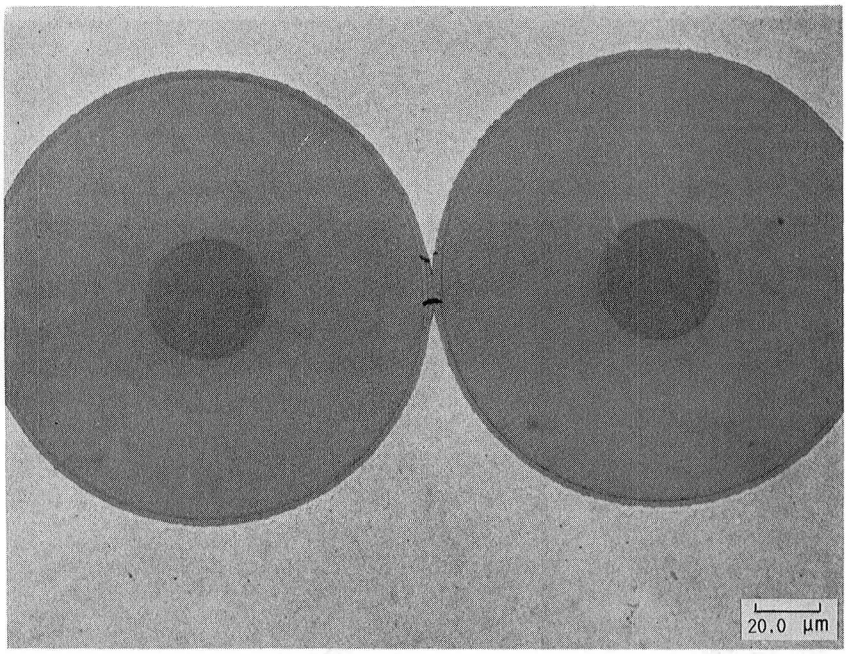


FIGURE 2. - CRACKS IN CARBON-RICH COATINGS OF TWO TOUCHING FIBERS (AS-POLISHED).

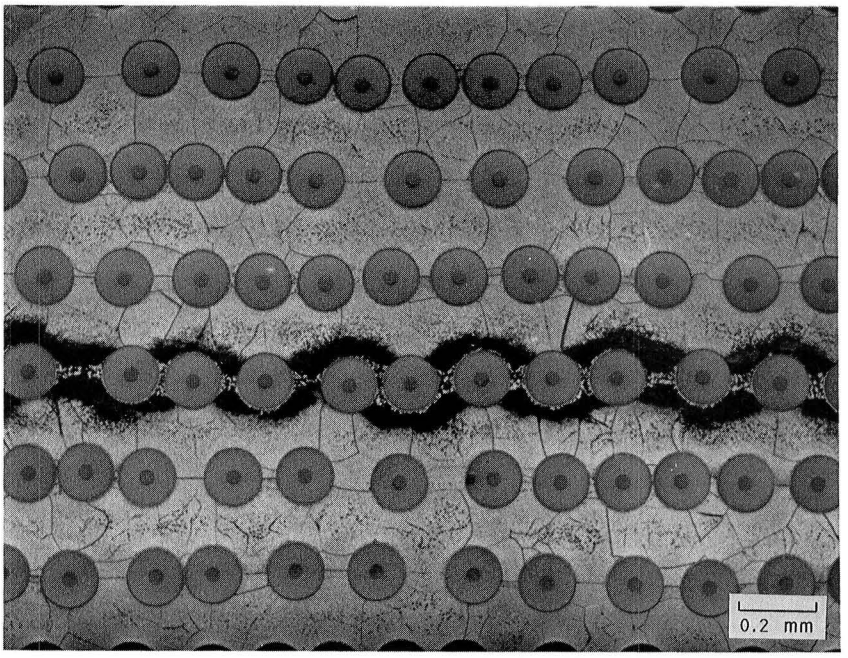


FIGURE 3. - RECTANGULAR GRAIN STRUCTURE IN TRANSVERSE PLANE OF COMPOSITE (SPECIMEN POLISHED AND ETCHED).

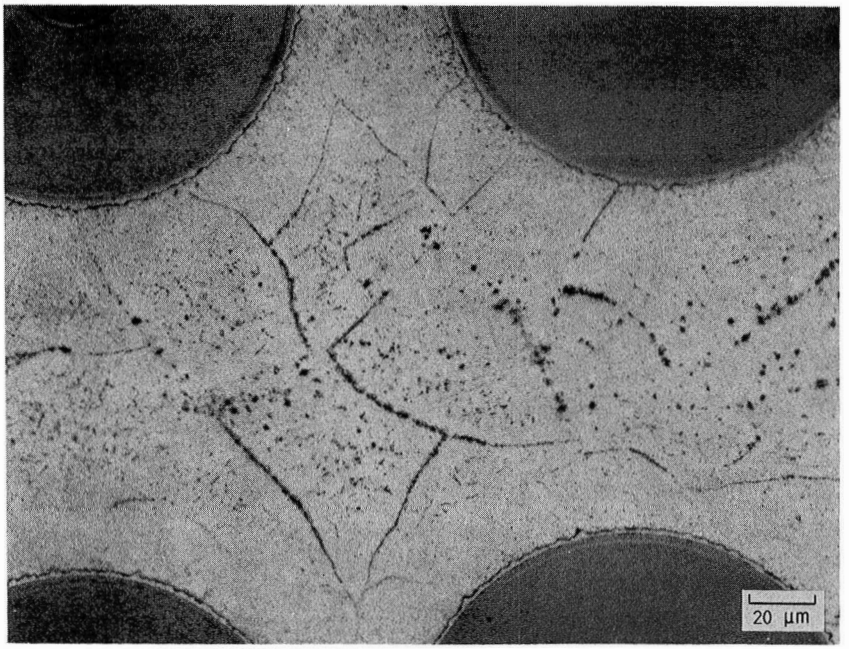


FIGURE 4. - SUBGRAINS IN Ti-15-3 MATRIX (SPECIMEN POLISHED AND ETCHED).

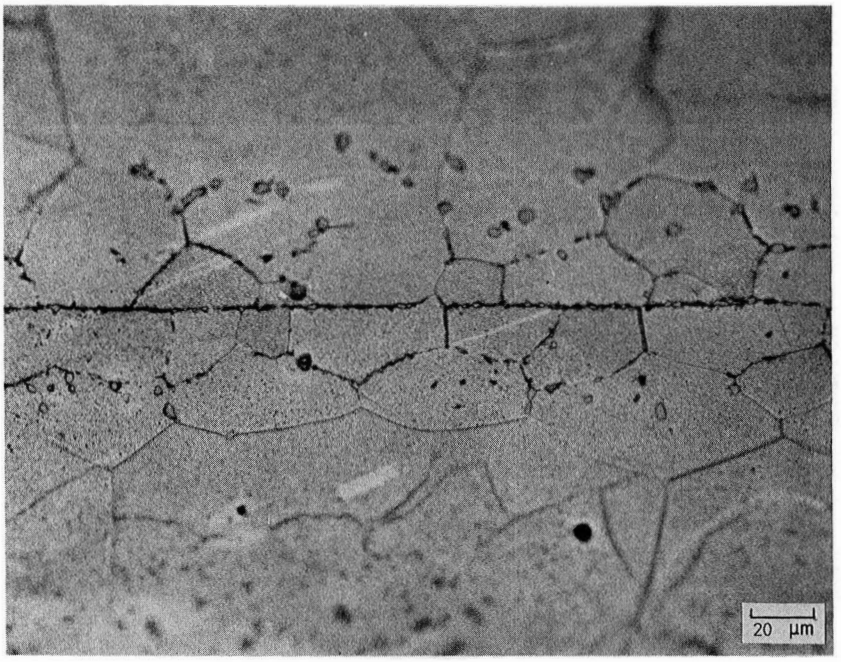


FIGURE 5. - SMALL GRAINS ADJACENT TO A FIBER SHOWN AFTER FIBER HAS BEEN POLISHED THROUGH (SPECIMEN POLISHED AND ETCHED).

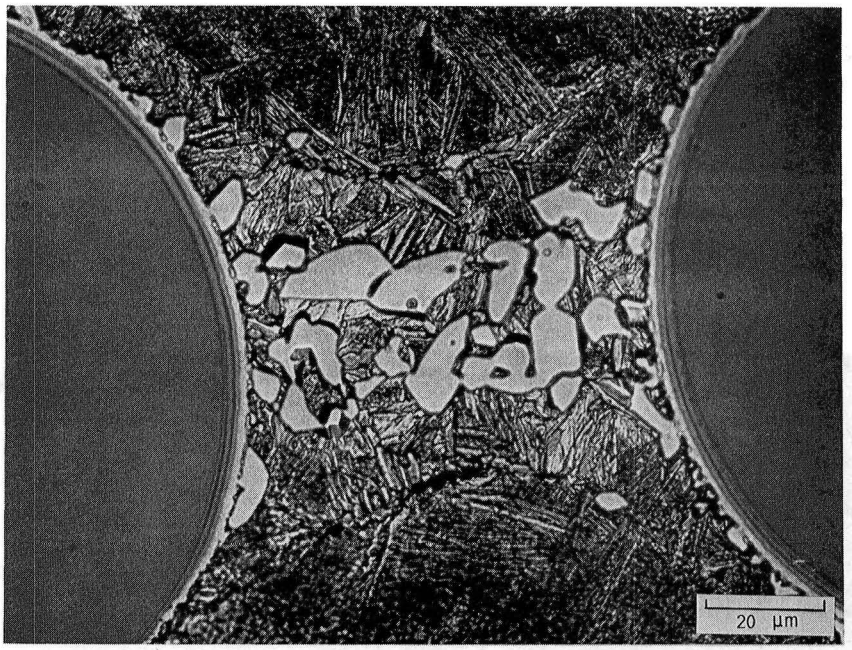


FIGURE 6. - LARGE, WHITE PARTICLES OF TiC AND α-β LAMELLAR STRUCTURE FORMED FROM Ti WIRE WOVEN BETWEEN FIBERS PRIOR TO CONSOLIDATION (SPECIMEN POLISHED AND ETCHED).

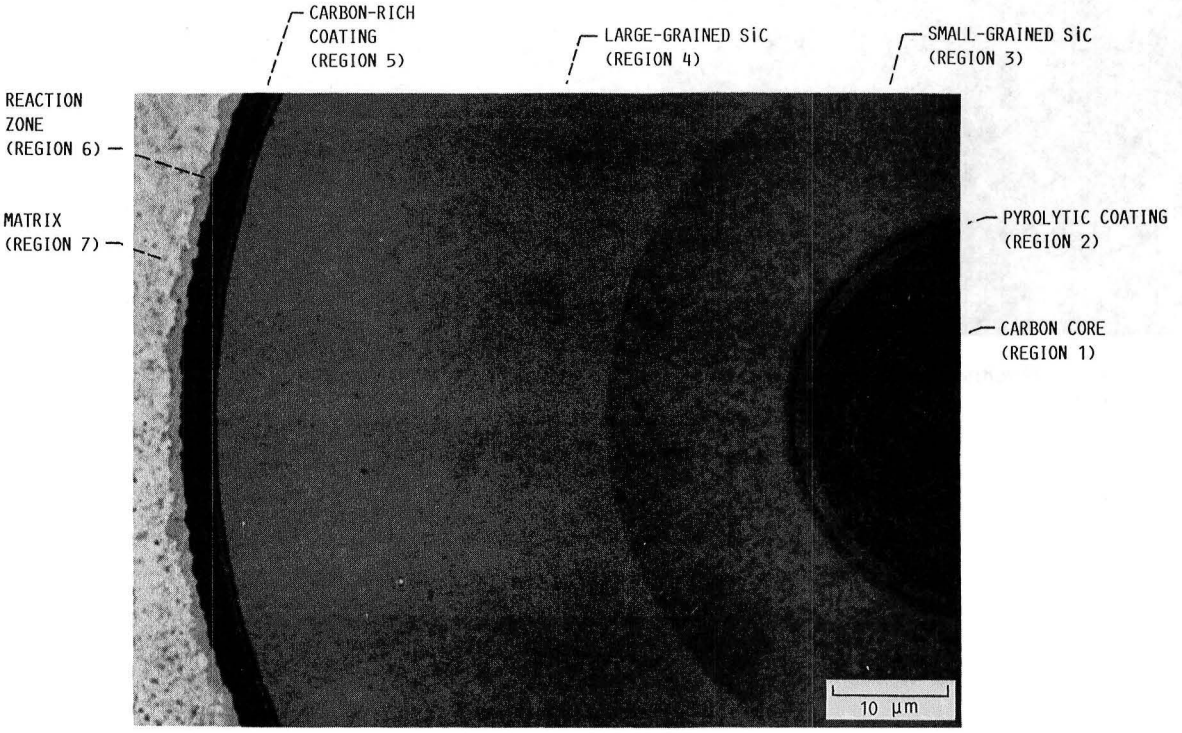


FIGURE 7. - PORTION OF FIBER IN POLISHED AND INTERFERENCE-LAYERED CONDITION SHOWING REGIONS 1 TO 7.

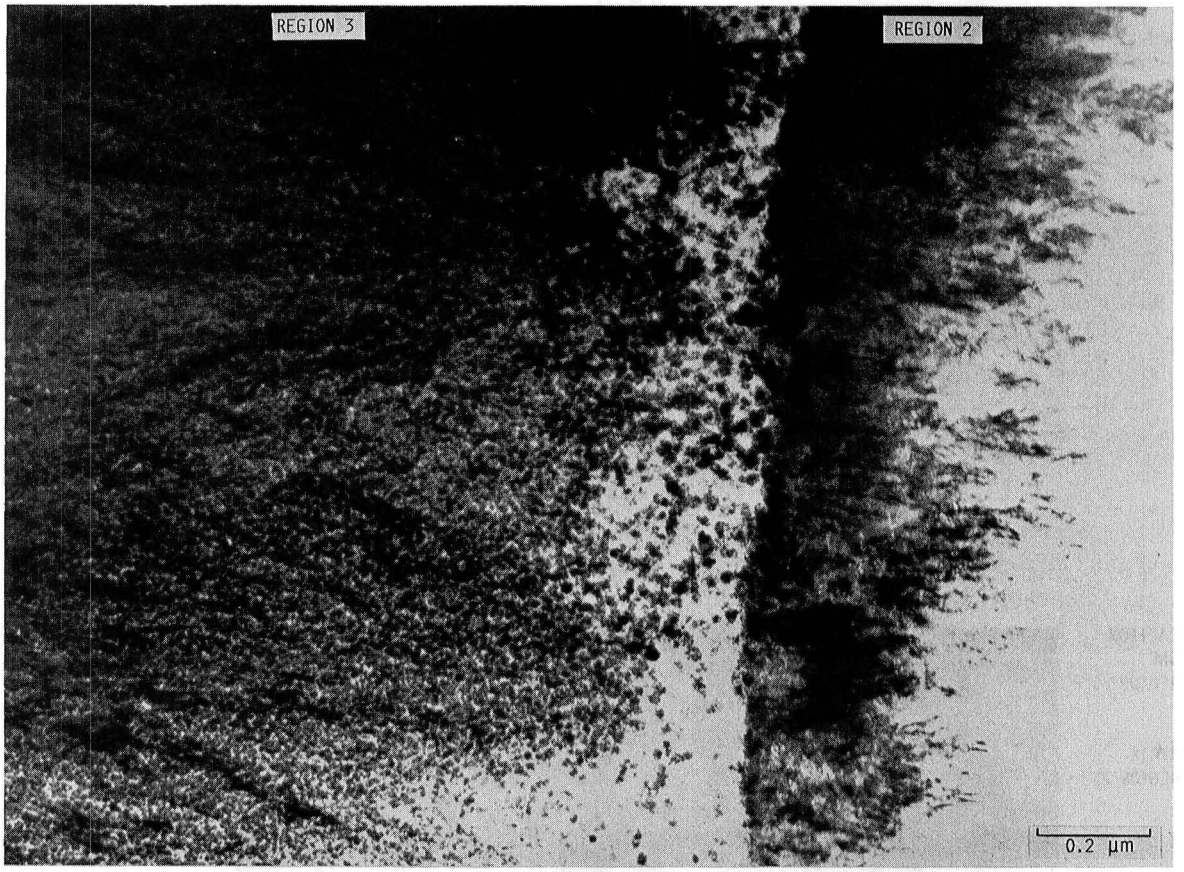


FIGURE 8. - TRANSMISSION ELECTRON MICROSCOPE (TEM) MICROGRAPH OF PYROLYTIC COATING (REGION 2) AND SMALL-GRAINED SiC (REGION 3).


(A) LARGE, ELONGATED GRAINS CONTAINING STACKING FAULTS.

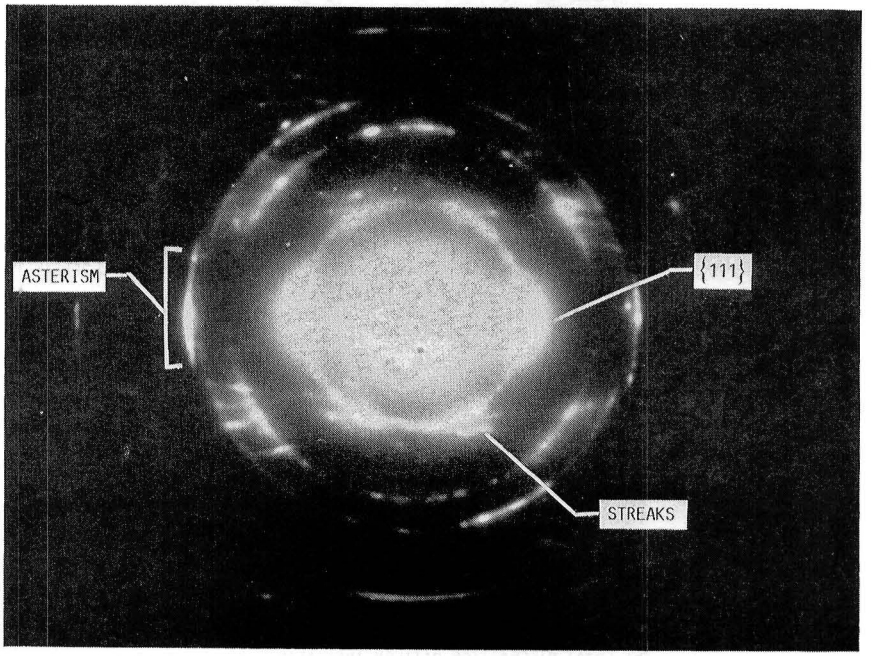


(B) DIFFRACTION PATTERN OF AREA IN FIGURE 9(A).

FIGURE 9. - TRANSMISSION ELECTRON MICROSCOPE (TEM) MICROGRAPH OF LARGE-GRAINED SiC (REGION 4) AND DIFFRACTION PATTERN.

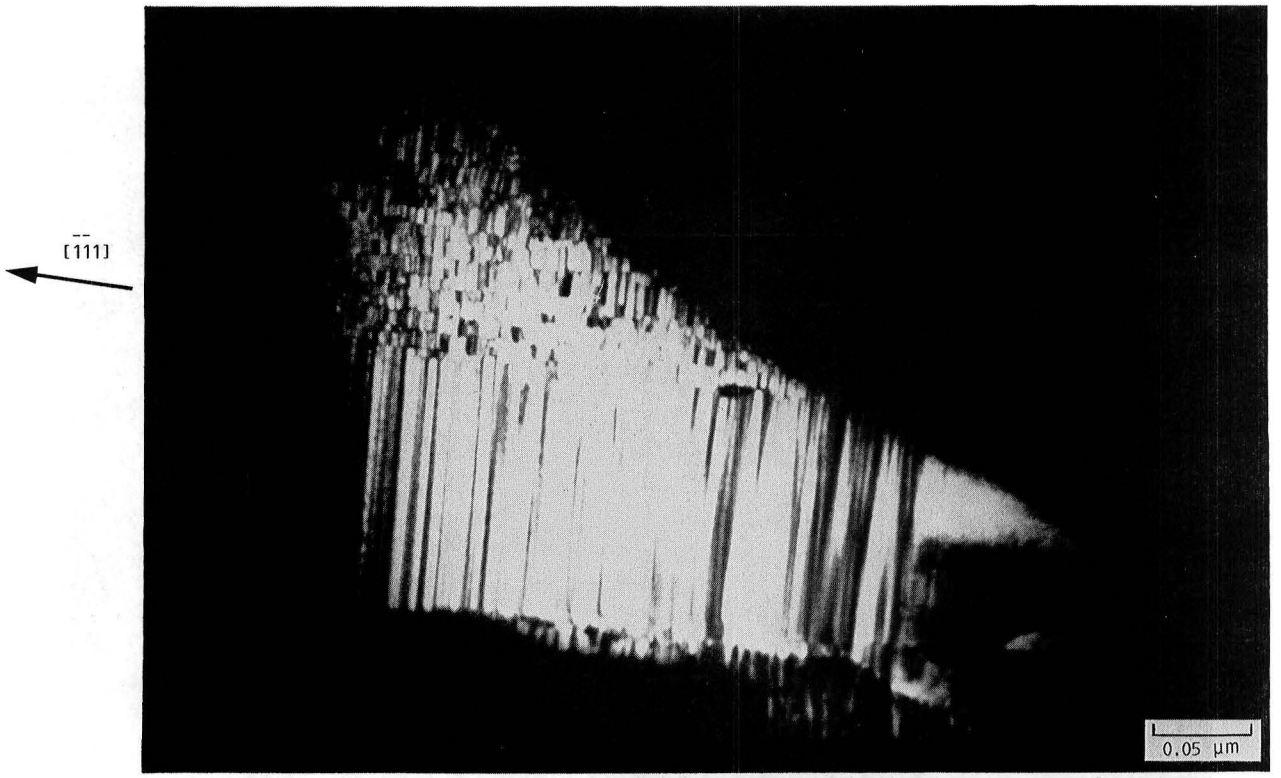


(A) DARK FIELD MICROGRAPH OF SiC GRAIN (FAULTS EDGE-ON).

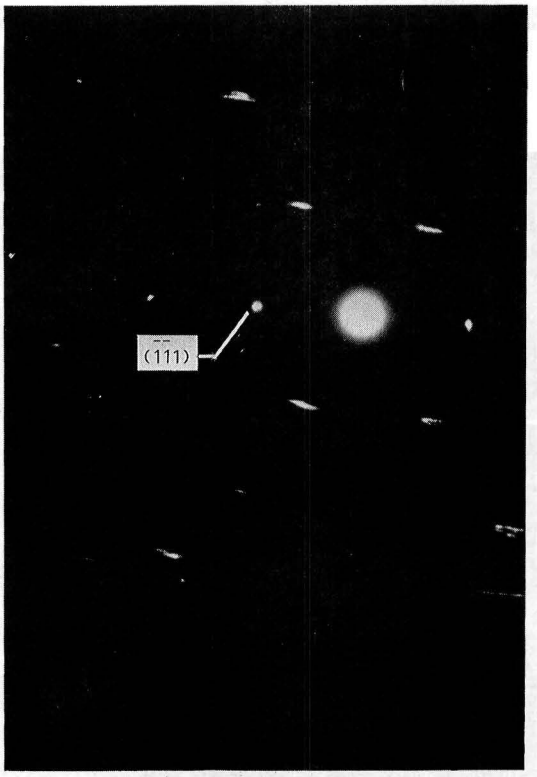


(B) [011] DIFFRACTION PATTERN INDICATING <111> DIRECTION PARALLEL TO GROWTH DIRECTION OF GRAIN.

FIGURE 10. - DARK FIELD MICROGRAPH OF ONE SiC GRAIN (REGION 4) AND DIFFRACTION PATTERN.

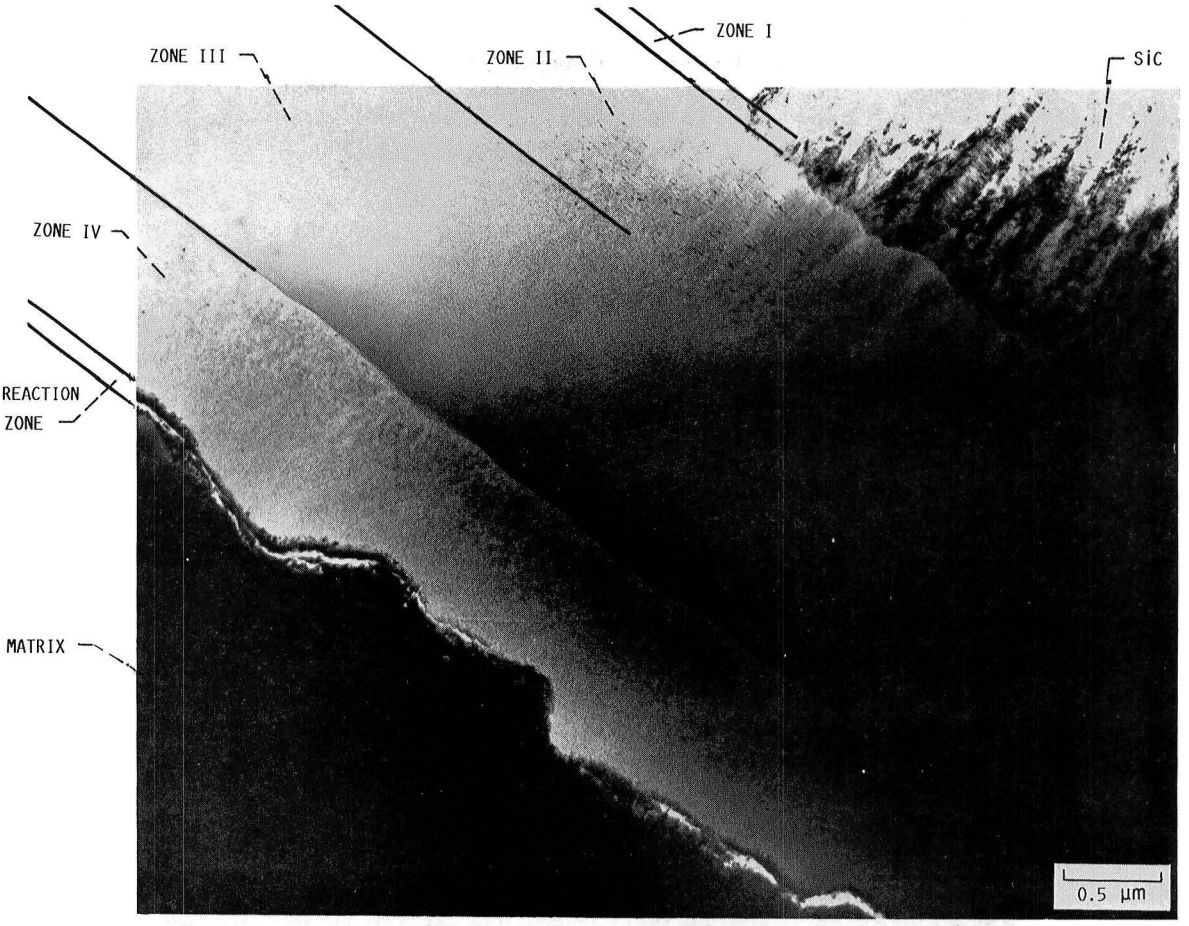


FIGURE 11. - TEM MICROGRAPH OF VARIOUS ZONES WITHIN CARBON-RICH COATING (REGION 5) AT FIBER/MATRIX INTERFACE.

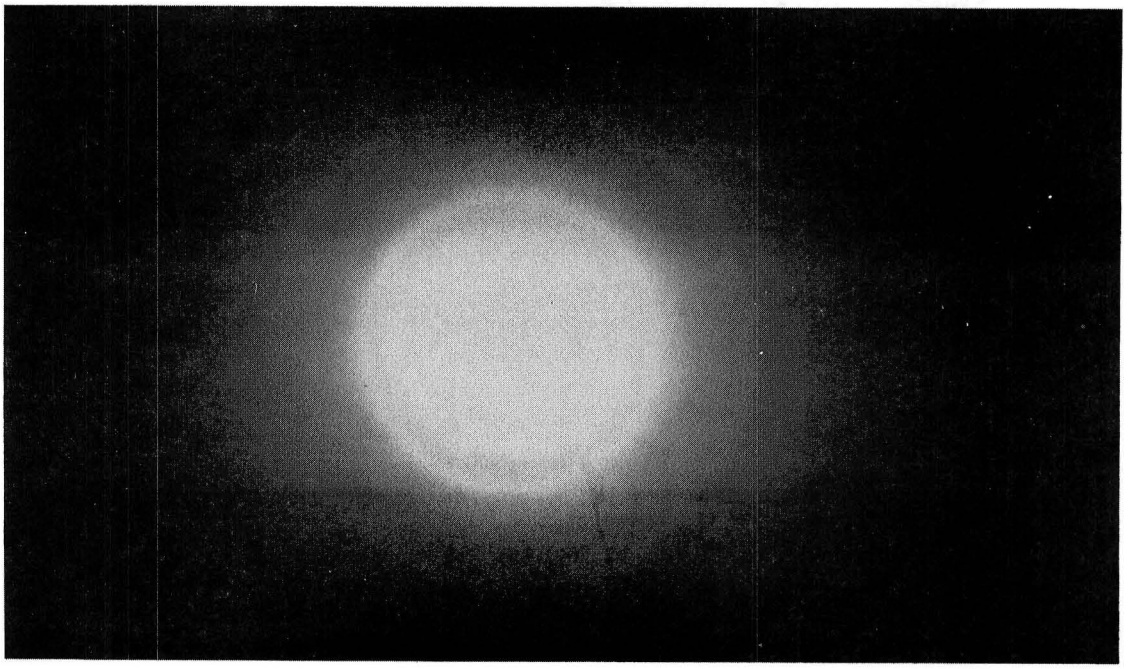

FIGURE 12. - DIFFRACTION PATTERN SHOWING AMORPHOUS STRUCTURE IN ZONE III OF CARBON-RICH COATING.

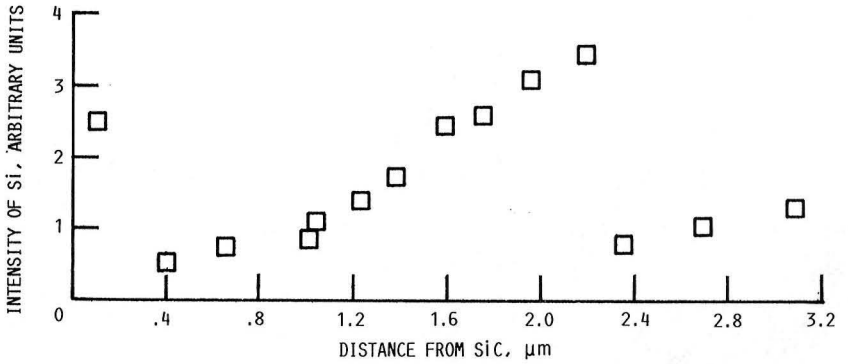


(A) SILICON CONTENT AS FUNCTION OF POSITION WITHIN CARBON-RICH COATING.

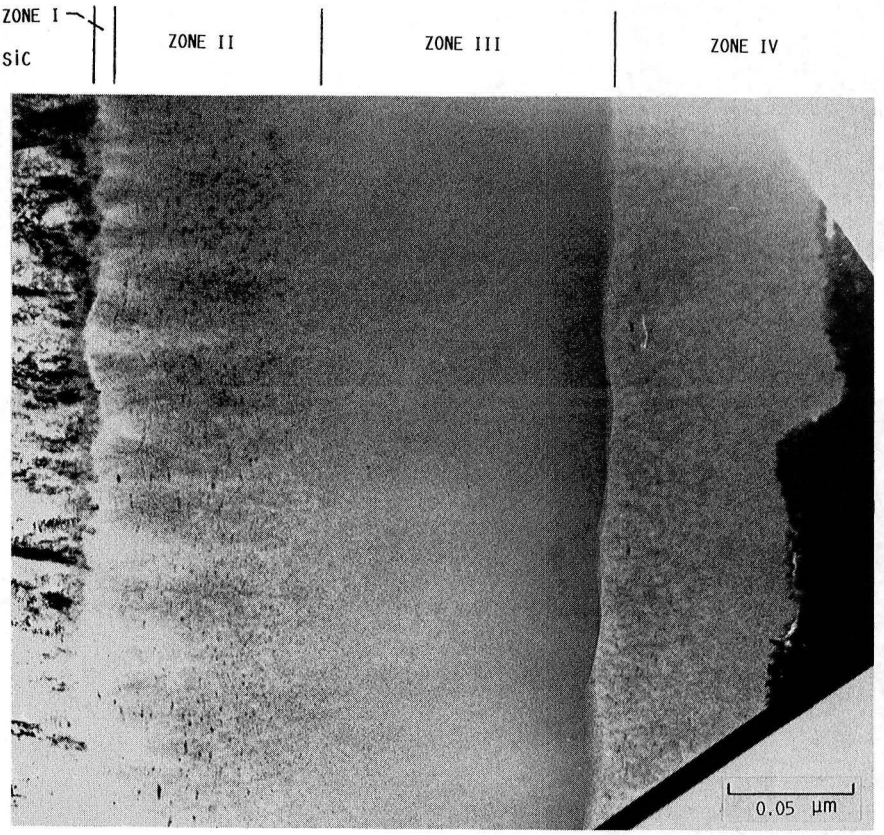


(B) BRIGHT FIELD MICROGRAPH.

FIGURE 13. - ELEMENTAL ANALYSES FOR SILICON CONTENT IN CARBON-RICH COATING (REGION 5).


(A) SMALL CRYSTALLITES WITHIN REACTION ZONE.

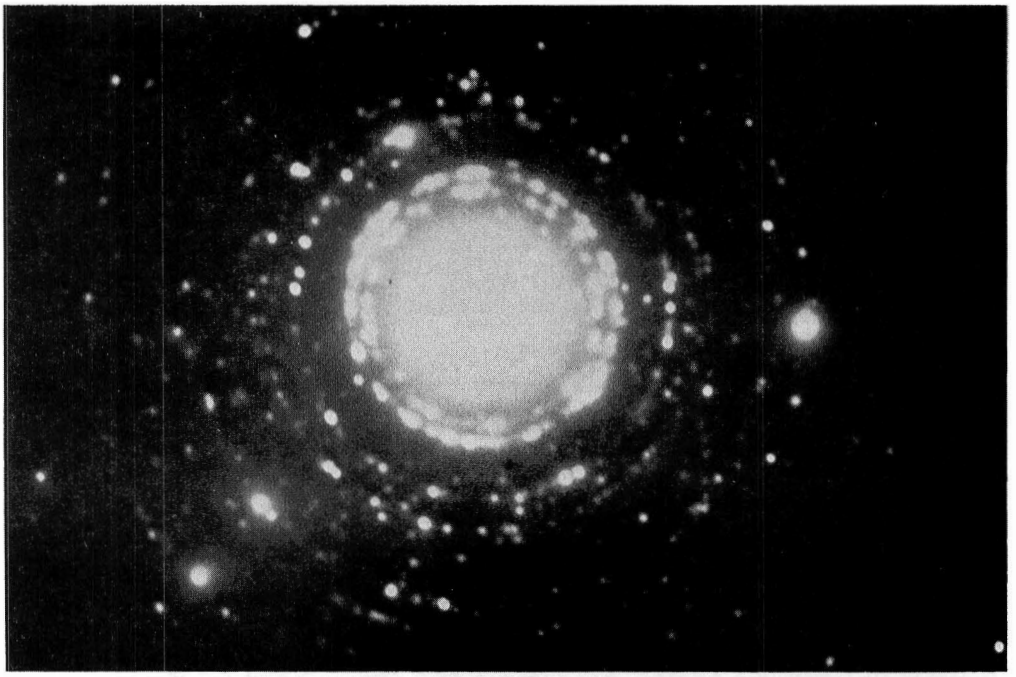

(B) COMPLEX DIFFRACTION PATTERN OF REACTION ZONE AS A RESULT OF VARIOUS ORIENTATIONS AND CRYSTAL STRUCTURES OF MINUTE GRAINS.

FIGURE 14. - TEM MICROGRAPH OF REACTION ZONE (REGION 6) AND DIFFRACTION PATTERN.

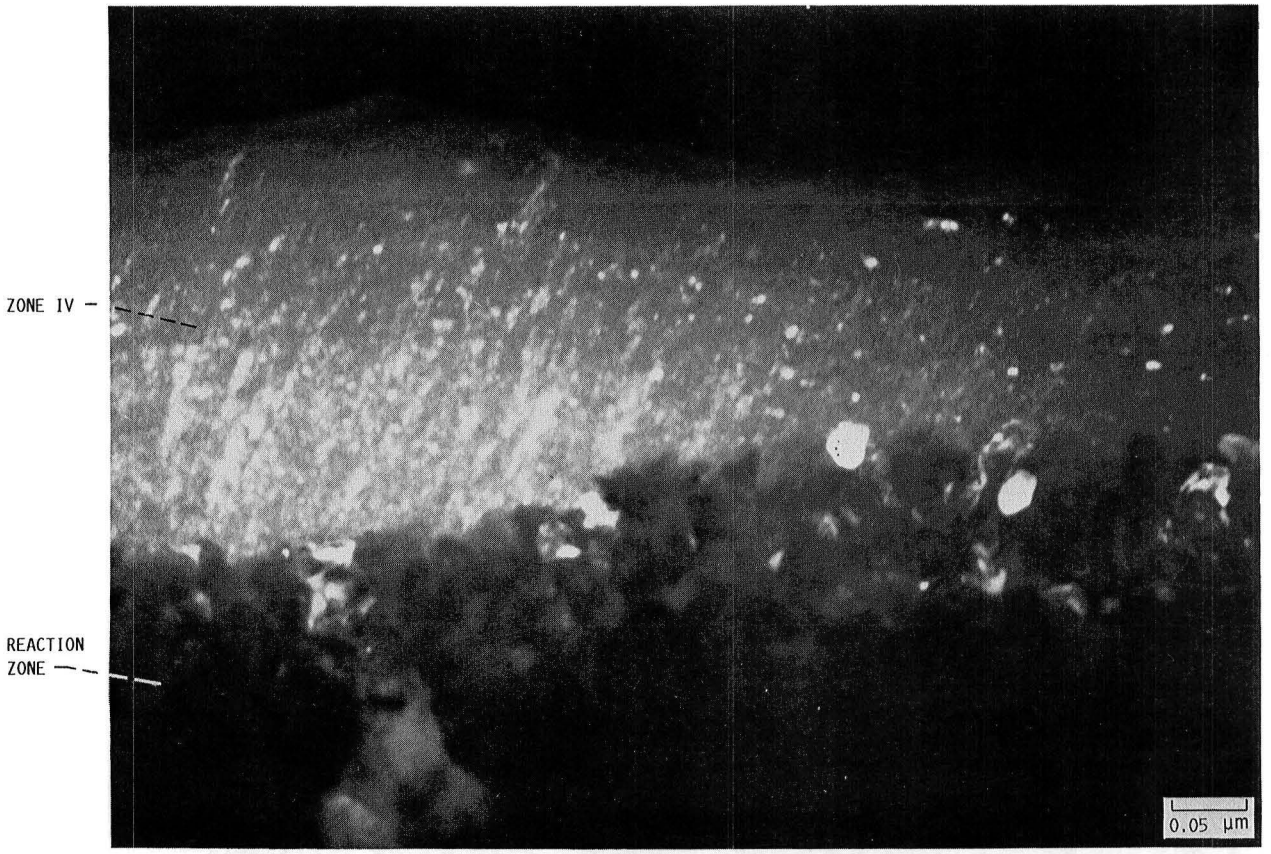


FIGURE 15. - DARK FIELD MICROGRAPH OF SMALL PARTICLES OF TiC WITHIN OUTER PORTION (ZONE IV) OF CARBON-RICH COATING.

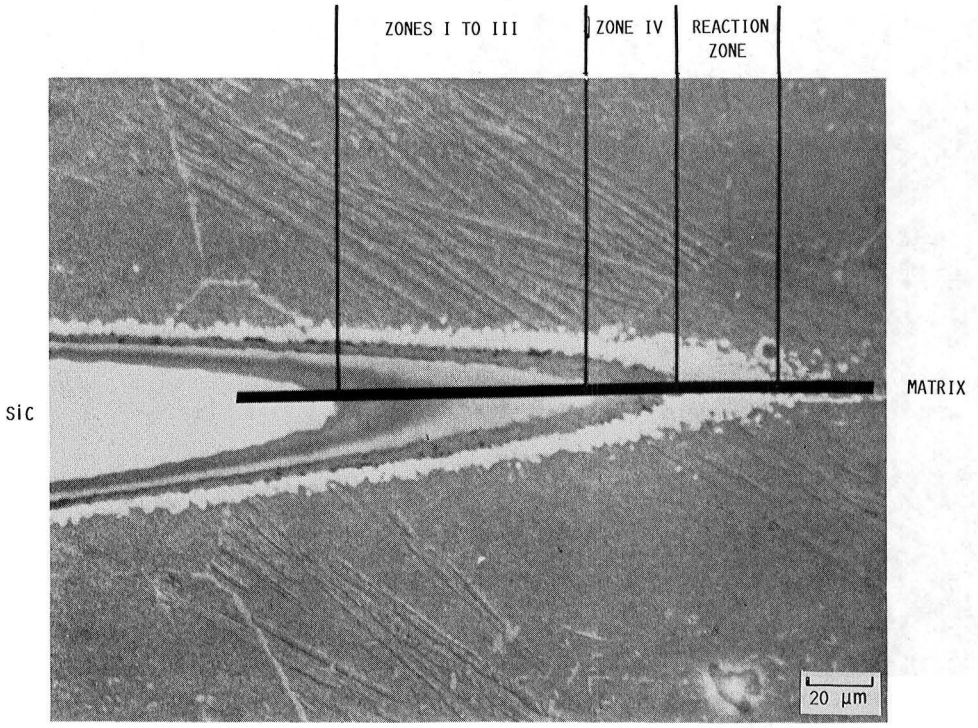


FIGURE 16. - TRACE OF MICROPROBE ANALYSIS ACROSS FIBER WHICH WAS SECTIONED OBLIQUELY TO EXAGGERATE SIZE OF INTERFACE AREA (INTERFENCE LAYERED).

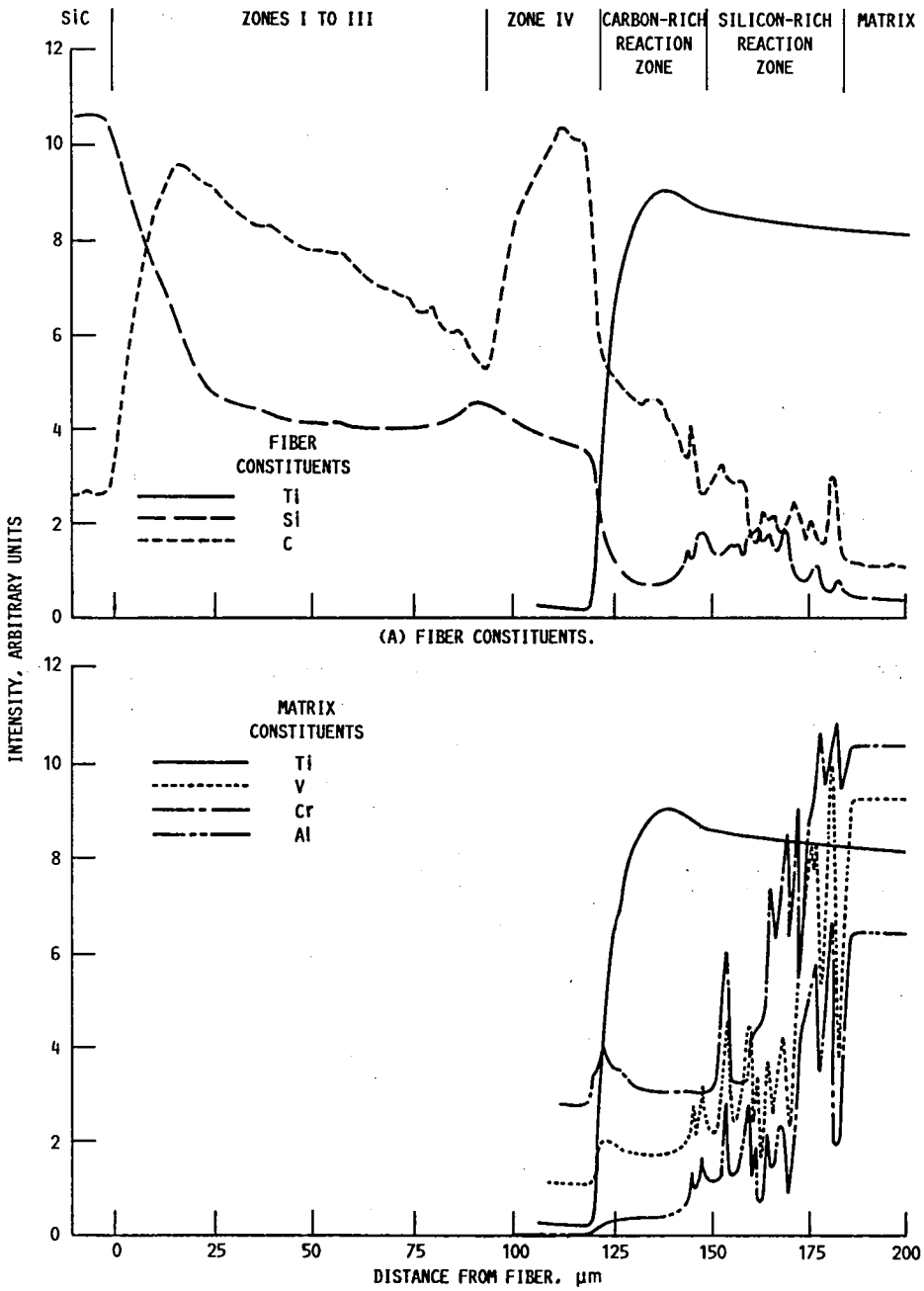


(A) FIBER CONSTITUENTS.

(B) MATRIX CONSTITUENTS.

FIGURE 17. - ELEMENTAL X-RAY INTENSITY AS FUNCTION OF POSITION (MICROPROBE ANALYSIS).

NASA
National Aeronautics and Space Administration

# Report Documentation Page

| 1. Report No. | 2. Government Accession No. | 3. Recipient's Catalog No. |
|---|---|---|
| NASA TM-100938 | | |

| 4. Title and Subtitle | 5. Report Date |
|---|---|
| As-Received Microstructure of a SiC/Ti-15-3 Composite | August 1988 |
| | 6. Performing Organization Code |

| 7. Author(s) | 8. Performing Organization Report No. |
|---|---|
| Bradley A. Lerch, David R. Hull, and Todd A. Leonhardt | E-4218 |
| | 10. Work Unit No. 535-07-01 |

| 9. Performing Organization Name and Address | 11. Contract or Grant No. |
|---|---|
| National Aeronautics and Space Administration<br>Lewis Research Center<br>Cleveland, Ohio 44135-3191 | |
| | 13. Type of Report and Period Covered: Technical Memorandum |
| 12. Sponsoring Agency Name and Address | 14. Sponsoring Agency Code |
| National Aeronautics and Space Administration<br>Washington, D.C. 20546-0001 | |

15. Supplementary Notes

Bradley A. Lerch and David R. Hull, NASA Lewis Research Center; Todd A. Leonhardt, Sverdrup Technology, Inc., NASA Lewis Research Center Group, Cleveland, Ohio 44135.

16. Abstract

A silcon carbide (SiC) fiber reinforced titanium (Ti-15V-3Cr-3Sn-3Al) composite is metallographically examined. Several methods for examining composite materials are investigated and documented. Polishing techniques for this material are described. An interference layering method is developed to reveal the structure of the fiber, the reaction zone, and various phases within the matrix. Microprobe and transmission electron microscope (TEM) analyses are performed on the fiber/matrix interface. A detailed description of the fiber distribution as well as the microstructure of the fiber and matrix are presented.

| 17. Key Words (Suggested by Author(s)) | 18. Distribution Statement |
|---|---|
| Ti-SiC; Ti-15-3; Composite metallography; Composite interface; Reaction zones; SCS-6 fibers; SiC/Ti | Unclassified - Unlimited<br>Subject Category 24 |

| 19. Security Classif. (of this report) | 20. Security Classif. (of this page) | 21. No of pages | 22. Price* |
|---|---|---|---|
| Unclassified | Unclassified | 26 | A03 |

NASA FORM 1626 OCT 86

*For sale by the National Technical Information Service, Springfield, Virginia 22161

NASA